2012-01-01

Magnetic Cell Separation by Inkjet Printing for Disease Monitoring

Sylvia Lucia Natividad
University of Texas at El Paso, slnatividad@miners.utep.edu

MAGNETIC CELL SEPARATION BY INKJET PRINTING FOR DISEASE MONITORING

SYLVIA LUCIA NATIVIDAD

Department of Metallurgical and Materials Engineering

APPROVED:

Thomas Boland, Ph.D., Chair

Mingtao Zeng, Ph.D.

Stephen Stafford, Ph.D.

Benjamin C. Flores, Ph.D.
Interim Dean of the Graduate School

Dedication

This thesis is dedicated to my wonderful family that I am so blessed to have.

MAGNETIC CELL SEPARATION BY INKJET PRINTING FOR DISEASE MONITORING

by

SYLVIA LUCIA NATIVIDAD, B.S. Metallurgical and Materials Engineering

THESIS

Presented to the Faculty of the Graduate School of

The University of Texas at El Paso

in Partial Fulfillment

of the Requirements

for the Degree of

MASTER OF SCIENCE

Department of Metallurgical and Materials Engineering

THE UNIVERSITY OF TEXAS AT EL PASO

May 2012

Acknowledgements

The University of Texas at El Paso

Department of Metallurgical and Materials Engineering

- Mr. David Brown
- Julio Rincon
- Maria Yanez
- Carlos Serna
- Dr. Stafford
- Dr. Boland

Texas Tech University Health Sciences Center

Center for Excellence in Infectious Diseases

Department of Biomedical Sciences

- Maria Arevalo
- Max
- Junwei
- Dr. Zeng

This material is based upon work supported by the National Science Foundation Graduate Research Fellowship under Grant No. 2011097659

Abstract

The standard analysis technique for cell sorting, flow cytometry, requires centralized facilities such as tertiary Medical Centers. According to the U.S. Department of Health and Human Services Designated Health Professional Shortage Areas (HPSA) Statistics, in this country alone, more than 35 million people live in medically underserved areas, many of which need access to diagnostic procedures for proper management of their diseases. A cell sorting technique that can be done in low-resource settings at a decreased cost to the medical organization and the patient has been developed through this research project. By combining inkjet printing technology and magnetic labeling of cells it is possible to obtain accurate cell counts needing only a regular optical microscope. Mouse spleen lymphocytes were mixed with anti-mouse CD4+ superparamagnetic microspheres and printed through a modified, commercial inkjet printer. The cells that bound to the magnetic labels landed on a polymer slide covering a permanent magnet while the rest of the sample was collected in an excess container for further analysis. The cell counts for this study were obtained by use of regular and inverted optical microscopes and open source imaging software developed by the National Institute of Health. Results from flow cytometry analysis of the "biological ink" are presented for comparison. This novel technique may improve upon existing technologies by reducing costs of training personnel, acquisition and maintenance of instrumentation, and time to conduct analysis.

Table of Contents

List of Tables

List of Figures

Chapter 1

Introduction

According to the World Health Organization (WHO), as of December 2010 approximately 34 million people are currently living with HIV/AIDS worldwide [51]. The data demonstrate that infectious diseases are still a global and national dilemma. Thus, in absence of effective vaccinations, treatment and management for these diseases are paramount. One way of managing infectious and chronic diseases such as HIV/AIDS, which specifically attacks CD4+ lymphocytes, involves expensive, bulky equipment that can only be used in specialized clinics and tertiary medical centers. This analysis technique, flow cytometry, can obtain a count of specified cells through immunofluorescent staining [3, 23, 26]. Here we employ a novel method for cell sorting and counting which is inexpensive, portable and has the potential to provide patients with point of care access to properly manage their disease. This new method has the potential to avail patients and laboratories with additional capabilities since it reduces the initial cost of equipment along with maintenance, transportation, and supply costs in comparison to other similar technologies [1].

The cell sorting process is done with a modified thermal inkjet printer that was originally manufactured to be light and portable. Thermal inkjet printing is desirable in cell sorting since it can dependably handle delicate biological material, it simplifies cell concentration calculations, and provides a semi-automated process that reduces the required skill level of the operator [8, 31, 54]. Two types of ink were used in this printing system. The first type of ink consisted of a mixture of blue non-magnetic and red magnetic microspheres that was used for a proof-of-concept study. The second biological ink was made of lymphocytes that were isolated from live mouse spleens and mixed with the paramagnetic microspheres. The surfaces of the paramagnetic microsphere are functionalized with antibodies specific to the CD4 receptor protein found on helper T cell membranes so that these lymphocytes are the only

ones that bind to the microsphere and become “magnetically labeled”. The magnetically labeled cells are sorted from the rest of the bio-ink when they are printed and collected for evaluation on a polymer microscope slide that is placed in front of a permanent magnet. The rest of the bio-ink, which consists of non-magnetically labeled cells, drains into an excess container. An open source imaging software program, FIJI, was used to analyze the images and obtain a cell count. The same cell populations as that used in the modified printer along with control samples were analyzed with flow cytometry for validation purposes and to obtain a reference standard for the approximate CD4+ lymphocyte content in a given spleen.

Chapter 2

Background

2.1 Global Health Disparity in Disease Diagnosis and Monitoring

Health disparity in disease diagnosis and monitoring is demonstrated by the prevalence of diseases throughout different regions in the world with varying levels of wealth. According to the World Health Organization (WHO) and UNAIDS there are about 34 million people living with HIV/AIDS in 2009 and 2010 worldwide. The WHO 2011 World Health Statistics report shows that in 2009 the rate of mortality due to AIDS is 163 per 100,000 people in countries that are considered to be low-income in comparison to the global rate of 33 per 100,000. The top ten countries with the most HIV/AIDS prevalence in 2009 are located in the African region where the average gross national income per capita (GNI per capita) is $2632 [36, 51]. Figure 2.1.1 demonstrates the differences between the Gross National Income per capita and % prevalence of HIV in adults aged 15-49 years in 2009 for these countries and three of the wealthiest countries in the world. The statistics from the WHO 2011 World Health Statistics shown in Figure 2.1.1 (a) and (b) demonstrate that these countries with the highest HIV prevalence are also economically underprivileged in comparison to the world's wealthiest countries that have a very low prevalence of HIV.

The availability of healthcare within a country is also an indicator of health disparities and the need for inexpensive, reliable medical technology alternatives. In Swaziland, the country with the highest prevalence of HIV in 2009, the average government healthcare expenditure per capita in 2008 was $86 and there were 1.6 doctors available per 10,000 people. In Malawi, the country with the lowest GNI per capita in Figure 2.1.1(a), government healthcare expenditure per capita in 2008 was $11 with 0.2 doctors per 10,000 people. In Switzerland, the wealthiest country in 2009, the average government healthcare expenditure per capita in 2008 was $4131 and there were 40.7 doctors available for every

10,000 people. In the U.S., the second wealthiest country in 2009, government healthcare expenditure per capita in 2008 was $3426 and there were 26.7 doctors available for every 10,000 people [51]. However, health disparity can also occur within a wealthy country such as the United States. The Office of Shortage Designation in the Bureau of Health Professions of the Health Resources and Services Administration (HRSA) U.S. Department of Health and Human Services reports that as of February 7th, 2012 an estimated 59,104,334 people live in designated Health Professional Shortage Areas (HPSA) throughout the United States [46]. All the states and U.S. territories have HPSA's within them and the estimated medically underserved population within these HPSA's is 35,079,801.Thus there is much evidence that demonstrates the need for low-cost point of care diagnostics that are portable, easy to use, and provide accurate results quickly in both underdeveloped and developed countries

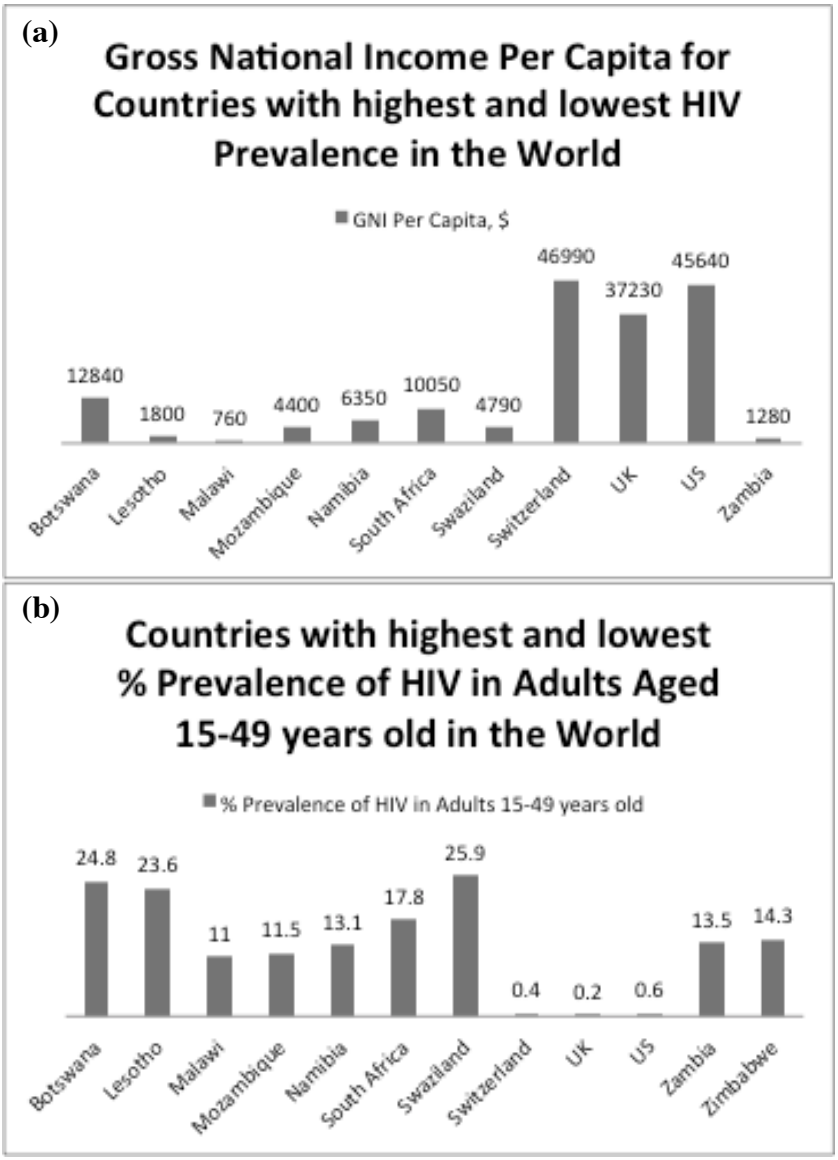

Figure 2.1.1: (a) GNI Per Capita for Countries with Highest and Lowest HIV Prevalence in 2009 (b) % Prevalence of HIV in Adults for Countries with Highest and Lowest values [51]

2.2 Global Market for Point of Care Diagnostics

According to the market research report by Kalorama Information on Point of Care Diagnostics for Emerging Infectious Disease Threats, there is a steadily growing market for low-cost, portable assays that are simple to use and can deliver fast, reliable results at the point of care site in low resource settings [35]. It has been determined that this is a consequence of the significant prevalence of infectious

and chronic diseases like HIV/AIDS throughout the world, especially in low resource settings both in developed and underdeveloped countries. Furthermore, these low resource settings in underdeveloped countries are usually located in remote communities that are dependent on nurses and trained medical personnel for treatment. This makes it necessary for the patients to obtain reliable results at the point of care (POC) site since there is no guaranteed follow-up visit. Such results also allow proper medical treatment to be administered at the POC and avoid drug resistant mutations of the disease. Kalorama Information estimates the market for diagnosing, monitoring, and treating infectious diseases in developing countries to grow from $132 million in 2010 to $246 million in 2015. In 2010 HIV/AIDS specifically, had a $200 million market in POC assays worldwide and approximately $30 million in developing countries, which is estimated to grow to about $50 million in 2015. [36]

Several nonprofit international programs exist that provide funding for research, diagnostic equipment, and treatment of HIV/AIDS. These include the United States President's Emergency Plan for AIDS Relief, the Gates Foundation, the Clinton Foundation, and the Global Fund to fight AIDS. The Joint United Nations Programme on HIV/AIDS (UNAIDS) estimated that approximately $15.9 billion was donated to the global HIV/AIDS response in 2009 by private donors in these organizations and governments; this is estimated to increase to $26 billion by 2015. In addition, many international agencies such as WHO, UNICEF, CARE, and USAID collaborate with local government programs to directly procure diagnostic equipment [36].

2.3 Human Immunodeficiency Virus (HIV)

Human immunodeficiency virus (HIV) is a retrovirus that attacks cells expressing the CD4 protein on their outer membrane surface, or CD4 positive (CD4+) cells. The virus core consists of two identical strands of viral RNA along with three enzymes, integrase, protease, and reverse transcriptase that are all encapsulated by a protein layer called a capsid. The core is then surrounded by a

phospholipid bilayer that contains two glycoproteins on the outer surface that are important in allowing the virus to interact with host cells. The outermost glycoprotein, GP120, has a high affinity for the CD4 protein and binds to cells expressing it on their membrane surface. The second glycoprotein, GP41, allows the viral membrane the host cell's membrane to fuse together so the virus can enter. Once inside, reverse transcriptase converts the viral RNA to viral complementary DNA (cDNA) which then enters the nucleus with the help of integrase. The virus RNA and necessary proteins are made by the host cell and released from the nucleus. The virus particles are then assembled into their capsids which undergo exocytosis and bud out of the host while using part of its membrane for the viral lipid bilayer. Lysis, or cell rupture, occurs once the new virus leaves the host cell. Therefore, the virus uses host cells to replicate and kills them once it is finished. [3, 23, 38]

HIV predominately affects CD4+ T lymphocytes since they express the highest levels of the CD4 protein. However, macrophages, monocytes, and dendritic cells, which are also white blood cells of the immune system, can also be targeted since they sometimes have low levels of CD4 expression. These latter cells do not lyse after HIV infection and serve as virus carriers that travel throughout the body. As a result, the standard form for monitoring the evolvement of HIV to acquired immunodeficiency disorder (AIDS) is through the measurement of a patient's CD4+ lymphocyte content which becomes progressively lower. As the CD4+ lymphocyte content drops, a patient's immune system becomes increasingly compromised and they develop AIDS. Knowing the CD4+ cell content also allows medical personnel to provide the necessary amount of antiretroviral medication (ART) to the patient and estimate their susceptibility to other infections. It is necessary to note that CD4+ cell counts are not used to initially diagnose a patient with HIV. Immunoblot tests or immunoassays such as Western Blot and Enzyme-Linked immunosorbent assay (ELISA) incorporate HIV antigens that are bound to a substrate such as nitrocellulose or polystyrene to detect the specific antibodies (or proteins) produced by an infected person [immunology and HIV Essentials]. HIV is also diagnosed with viral load assays such as

Polymerase Chain Reaction (PCR) or Reverse Transcriptase – Polymerase Chain Reaction (RT-PCR) that measure the amount of virus RNA present in a patient's blood plasma [HIV essentials]. These initial tests along with CD4+ cell counts are used to provide patients with proper management of their disease and a better quality of life. [3, 15, 38, 40]

2.4 Flow Cytometry

Flow cytometry is a fluorescent-activated cell sorting (FACS) technique that involves immunofluorescent staining of specific cells within a biological sample. Antibodies that are covalently bound to a fluorescent stain such as fluorescent isothiocyanate (FITC) or phycoerythrin (PE) are mixed with a biological sample where they bind to cells expressing their corresponding antigen. The "stained" sample is then run through a flow cytometer machine where cell identification is done with ultraviolet laser beams and a detector. The main components of a flow cytometer are one or more laster light source, forward scatter detector, side scatter detectors, hydraulic flow cell system, and a computer system. The biological sample is sent through the hydraulic flow cell where a sheath fluid is used to hydrodynamically focus the cells so that they pass through the incident laser one at a time. The laser beam causes the cell-bound fluorescent label to fluoresce and scatter light in all directions. The forward scatter detector, which is placed directly in front of the incident beam, detects the light scattered in the forward direction at about 0.5° to 10° to the laser axis. This scattered light is proportional the square of a sphere's radius and can provide a qualitative evaluation on the relative sizes of the cells. The side scatter detectors, placed at a right angle to the incident beam, detect the light scattered from the organelles within the cell and the intensity of the fluorescence from the marker. This scattered light is proportional to the granularity of the cell and provides a qualitative evaluation of the relative textures of the cells. The photons that land on the detectors are converted to an electric current which is amplified by a photo multiplier (PMT). This amplified signal is then converted to a with an analog-to-digital converter for analysis with a computer system. The computer system obtains the intensity and quantity of scattered

light and the data can be displayed in histograms or density plots. The histogram shows the event counts, or cells, as a function of the fluorescent light intensity. The density plots demonstrate the side scatter light intensity as a function of the forward scatter light intensity. These plots allow for the identification of different cell types since each dot is a single cell and both the size and granularity can be seen. [3, 26]

2.5 Superparamagnetic Microspheres for Cell Sorting

Superparamagnetic microspheres for cell sorting use affinity ligands that are conjugated to their surface in order to isolate specific cell types from a biological sample [13, 16, 17, 18, 20, 28, 39,44,49]. The microspheres are composed of a porous, polystyrene core that is embedded with magnetic iron oxide particles. They are prepared by aqueous emulsion polymerization in an "activated swelling" method that begins with monosized styrene seeds. The polymer seeds are activated and polymerized by absorbing vinyl monomers and then swollen with slightly water insoluble compounds such as toluene. The latter component is also a porogen that leaves behind pores throughout the swollen microsphere's surface once it is extracted. Monosized, porous polymer microspheres are the result of this processing method. The pores are then coated with $-NO_2$ or $-ONO_2$ so that they become hydrophilic and immediately fill up with liquid when placed in an aqueous solution of Fe^{2+} salts. Heating the microbeads causes the formation of small grains of iron oxide within the pores that are between 20 to 40 nm in diameter. The microbeads are then coated with a hydrophobic polymer that fills up the pores and provides the surface on which ligands can bind. The most common polymer used for this coating is epoxy resin [17]. The ligands thiol (R-SH), hydroxyl (R-OH), or amine groups ($R-NH_2$) at their surface can be covalently bound directly to the epoxide functional group at the polymer surface through thioether, ether, or secondary amine bonds respectively. Ligands can also be bound to the microbeads through activation of secondary function groups [17, 18, 41]. This is the case for M-450 dynabeads that are used to make anti-mouse CD4 microbeads. The epoxy surface for these microbeads is activated with a tosyl functional group that covalently binds to primary amines or sulphydryl (thiol) groups. The

magnetically isolated cells can also be removed from the microspheres with the use of Sorbitol which replaces the bond between the antibody and the bead. This method nondestructively releases the cells from the beads after two hours of gentle agitation so they may be used for other analytical techniques. [17, 39].

The iron oxide formed within the microbead pores is maghemite, γ-Fe_2O_3, which is ferromagnetic and has a spinel crystal structure. Maghemite has 11% less iron than Magnetite. This creates vacancies and an unequal distribution of Fe^{3+} in the crystal lattice which results in ferrimagnetism. The overall superparamagnetic properties of the microbeads is achieved because each maghemite grain has its own magnetic dipole moment that is proportional to its volume [17]. Thus, the grains, or nanoparticles, have magnetic anisotropy in the absence of an external magnetic field so that the microbead exhibits non-magnetic behavior. However, when the external field is applied, the magnetic dipole moments of all the nanoparticles tend to align along the applied field and create a net magnetization for the microbead. In addition, the microbeads usually have little to no magnetic remanence since the removal of the external field renders the nanoparticles in their initial state. Due to these properties, the magnetic microspheres do not clump and can be homogenously suspended within a fluid biological sample [11, 27, 43].

The use of superparamagnetic microspheres in cell sorting is advantageous because they can reliably isolate a variety of specified cell types from a mixed sample without the use of expensive, bulky equipment. According to the manufacturer, dynabeads have an isolation purity of more than 95%. Thus, this cell sorting method is accurate, simple, and less expensive in comparison to technologies that perform the same function. As a result, this technique can be used in laboratories with very basic supplies and equipment. [1, 3, 17]

2.6 Available CD4+ Lymphocyte Rapid Count Tests for Resource Poor Settings

Several rapid tests for counting CD4+ T-lymphocytes in blood samples are currently on the market or under development. These include the NOW instrument by PointCARE Technologies (Marlborough, MA), PIMA by Alere (Waltham, MA), CyFlow miniPOC technology by Partec (Swedesboro, NJ), a patent-pending, semi-quantitative test by The Macfarlane Burnet Institute for Medical Research & Public Health (Melbourne, Australia), a portable cell counter by Daktari Diagnostics (Cambridge, MA), and Zyomyx Inc.'s POC technology (Hayward, CA). The fully automated NOW instrument by PointCare Technologies is designed to obtain CD4+ and percent CD4+ cell measurements in low resource settings along with providing the haemoglobin concentration of the sample. The instrument costs about $15,000 to $20,000 and each test is ten dollars. The PIMA has a disposable cartridge that contains dried reagents that do not require refrigeration and is inserted into a portable analyzer that can obtain CD4+ cell counts within 20 minutes from whole blood samples. The CyFlow miniPOC is based on flow cytometry principles, however, it comes with dried reagents for CD4+ cell distinction and is lightweight and portable for use in remote, low-resource settings. The test developed by The Macfarlane Burnet Institute for Medical Research & Public Health gives a semi-quantitative result that shows if the patient's CD4+ lymphocyte count is above or below 350 cells/mm which is the WHO's determination of when someone should begin antiretroviral therapy. Daktari Diagnostics has developed a battery operated CD4+ cell counter that consists of a sample carrying cartridge that is inserted into an analyzer that reads electrical signals and gives an absolute count within a few minutes. Zyomex's POC assay uses reagents that bind to CD4+ lymphocytes and move them to a region in the device where a cell count can be obtained visually, similar to a simple thermometer. [36]

Chapter 3

Experimental Details

3.1 Mouse Spleen Lymphocytes

The lymphocytes isolated from mice spleens were obtained from female mice strain BALB/cOLaHsd-Foxn1^{nu} (Harlan Laboratories, Houston, TX). The mouse spleens were mashed through a cell strainer with the plunger end of a syringe into a 50 ml conical tube. The cell strainer was then rinsed with 5 ml of DMEM-10 (Dulbecco's Modified Eagles Medium + 10% FBS + 1X Penicillin/Streptomycin) (Sigma Aldrich, St. Louis, MO). The cells were then centrifuged, the supernatant was discarded, and the cell pellets were resuspended in 1 ml ACK lysis buffer (Life Technologies, Grand Island, NY). The cells were allowed to incubate at room temperature for ten minutes after which 9 ml of DMEM-10 was added. The cells were then counted with a hemocytometer and viability was assessed by Trypan Blue exclusion.

3.2 Biological Ink

Initial testing consisted of an ink made of two types of microspheres. Polybead® Polystyrene Blue Dyed Microspheres (Polysciences, Warrington, PA) were mixed with superparamagnetic ProMag™ 3 Series COOH Surfactant-Free Microspheres (Polysciences) in a 3:1:6 ratio with deionized water. To create the biological ink, Invitrogen^{TM} anti-Mouse CD4 Dynabeads® (Life Technologies, Grand Island, NY) were prepared according to the manufacturer protocol. Prior to attachment, 25 µL of the beads were washed in 1 mL of isolation buffer which consisted of PBS with 0.1% BSA and 2 mM EDTA. The beads were then re-suspended in 1 mL of isolation buffer and added to the mouse spleen lymphocytes (splenocytes) and mixed gently. The complete sample was allowed to incubate for 20 minutes at 8°C with slow rotation to ensure a homogenous solution.

3.3 Printer Modification

A Hewlett-Packard Deskjet 340 thermal inkjet printer was modified to magnetically sort cells contained within the bio-ink in a semi-automated process (Fig. 3.3.1). Modifications to the printer include a lightweight, 6061 aluminum T6 frame with a customized printing platform that holds the permanent magnet and excess container. The printer is capable of printing at an arbitrary angle between vertical (Fig. 3.3.2) and horizontal positions (Fig. 3.3.3). The printing platform is adjustable in both forward and backward directions, which allows for flexibility in optimizing the distance between the modified ink cartridge to the permanent magnet. The permanent magnet configuration consists of two Neodymium rare-earth magnets. Both magnets are sintered $Nd_2Fe_{14}B$ Grade 42 with transverse magnetization and a Ni-Cu-Ni triple layer coating for corrosion resistance (Applied Magnets, Plano, TX, USA). The magnet to which the substrate slide is mounted is 4" x 1" x 0.5" and has an approximate pull force of 110 pounds. The secondary magnet is 2" x 1" x 1" with about 145 pounds of pull force. The ideal printing parameters and substrate were determined in the Proof-of-Concept study. The excess container is a BD Falcon polystyrene 60 x 15 mm petri dish (BD Biosciences, Bedford, MA).

The ink pens for the printer cartridge were modified to print the bio-ink by removing the original ink, thoroughly cleaning the cartridge, and inserting a 0.6 ml conical tube with openings on either end into the nozzle pen area. The range of volume that could be printed was set according to the cartridge capacity and printer firing settings. The pen has 50 nozzles with 54 μm diameters and droplet volume of 85 to 120 pl [2]. The volume of bio-ink loaded and printed during a single printout for a solitary slide was 20 μl. The printed samples were viewed under a Nikon Eclipse Ti inverted optical microscope (Nikon Instruments Inc., Melville, NY) and 2560 x 1920 pixel images with 0.34 μm/pixel resolution were taken using NIS-Elements AR imaging software (Nikon Instruments Inc., Melville, NY).

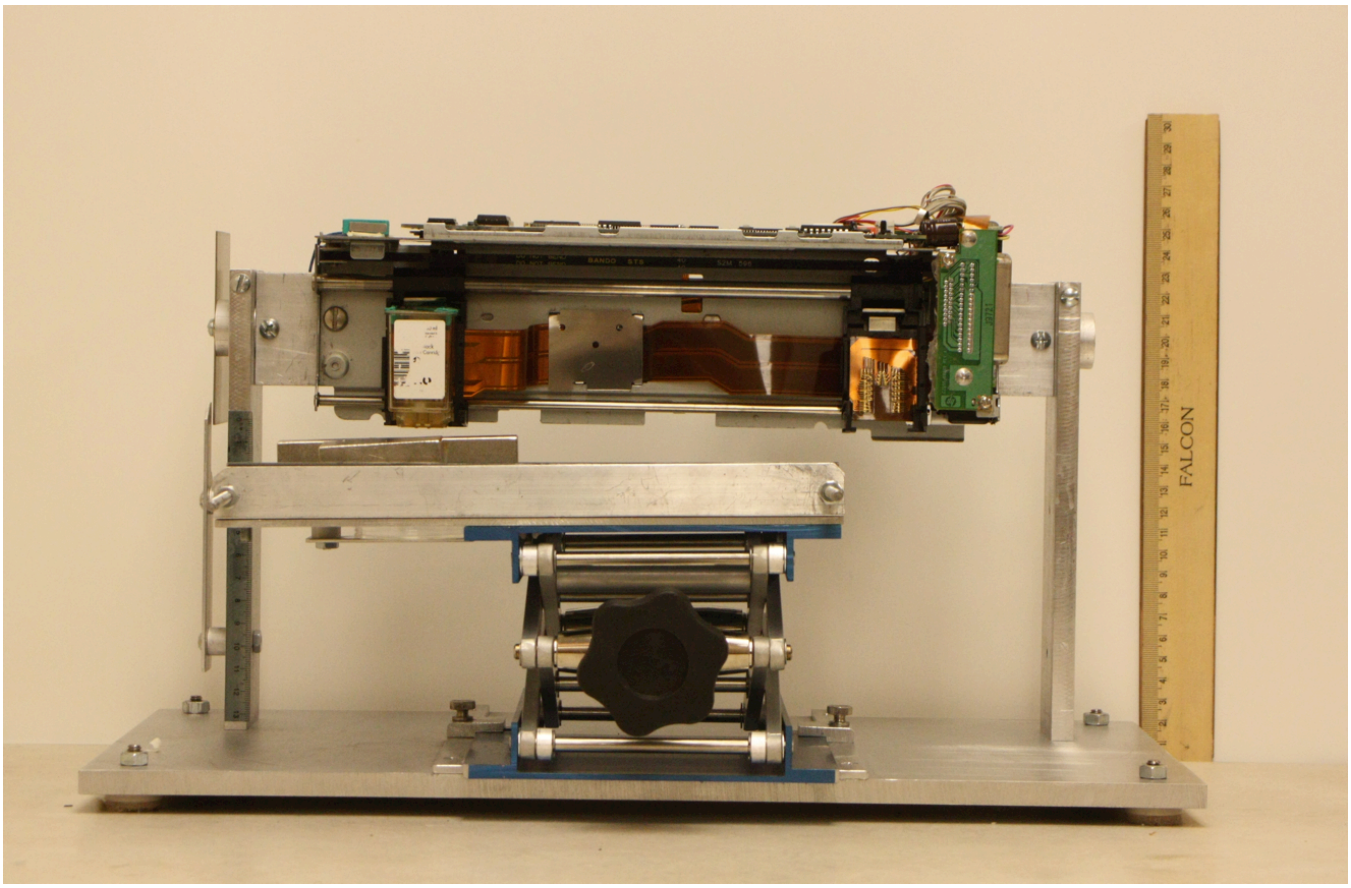

Figure 3.3.1: Cell Sorting Printing System

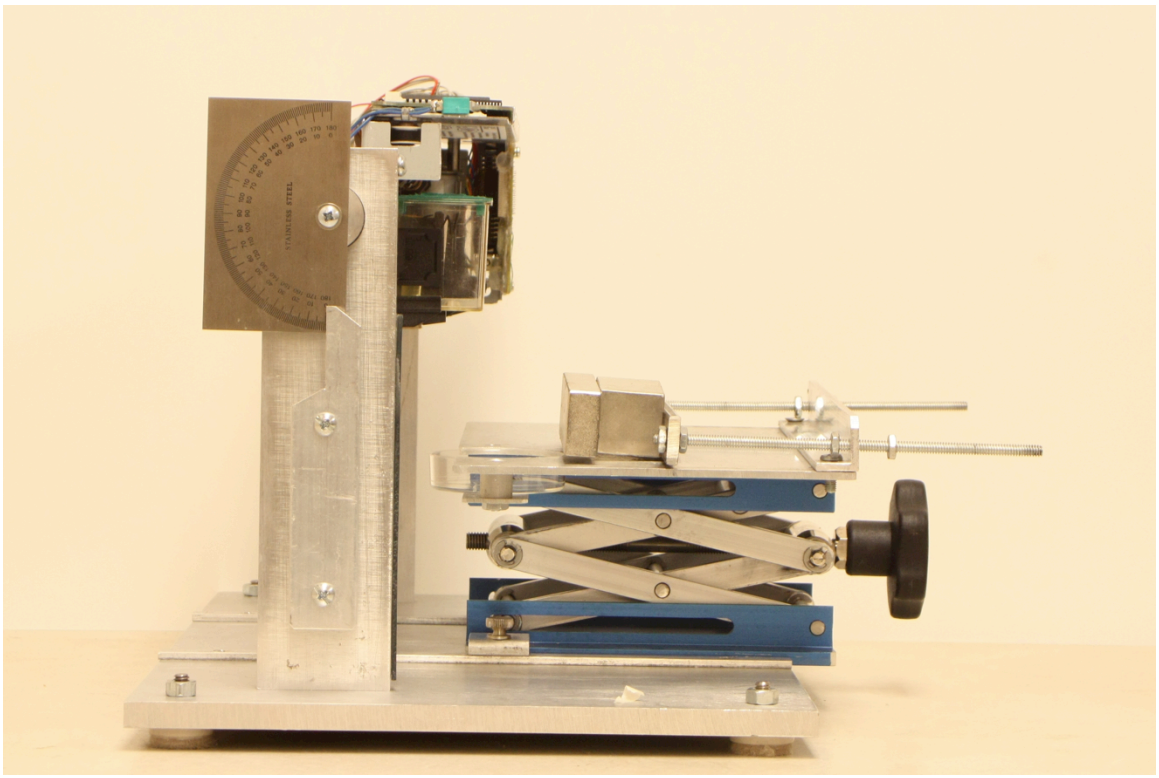

Figure 3.3.2: Cell Sorting Printing System: Vertical Position

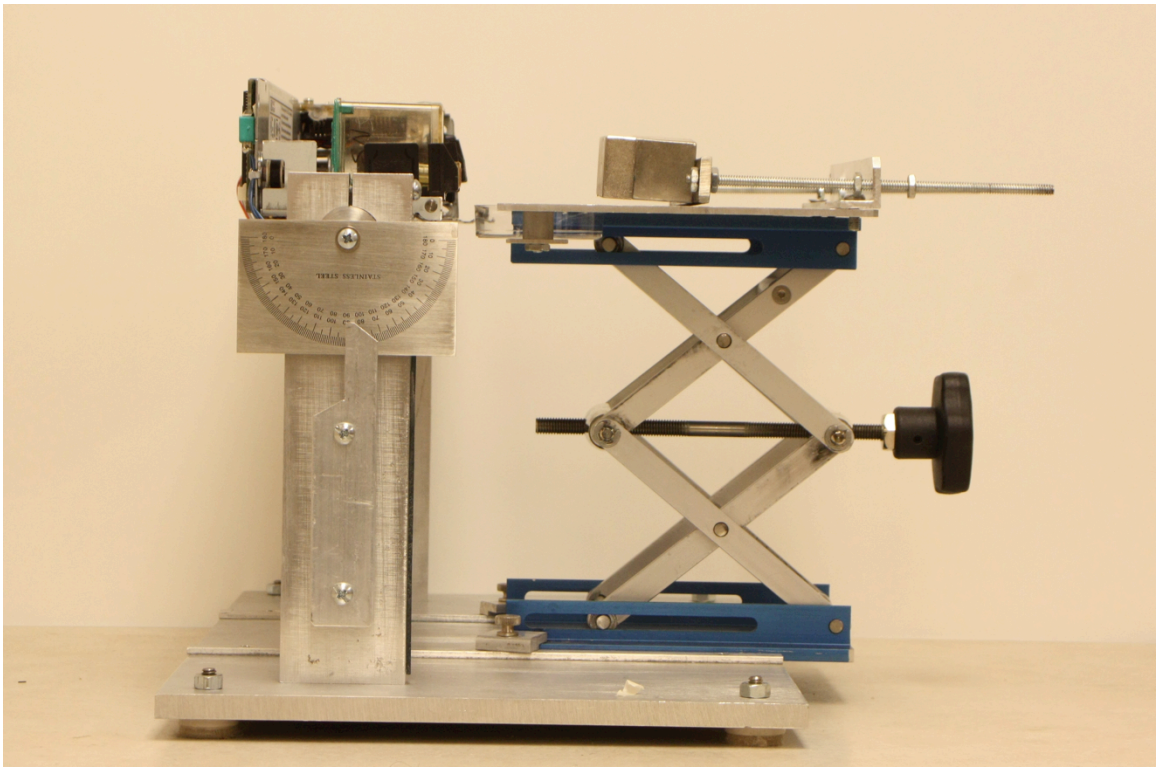

Figure 3.3.3: Cell Sorting Printing System: Horizontal Position

3.4 Printing Process

The optimized printing process begins once the bio-ink as been prepared and the modified printer is in the printing position where cell sorting occurs as was previously described. The excess container is then placed in its respective holder on the printing platform and filled with 2 ml of PBS. The polymer slide is then fixed to the permanent magnet with a double sided adhesive strip. The printer cartridge is then loaded with 20 µl of bio-ink and printed. The non-magnetically bound part of the bio-ink slides to the bottom edge of the polymer slide and is gently washed down into the excess container with a pipette filled with 0.5 ml PBS. In order to fixate and preserve the magnetically bound cells, the polymer slide is removed from the magnet and a drop of CC/Mount^{TM} Media (Sigma-Aldrich) is added. The sample is then covered with a glass coverslip and allowed to dry for analysis with optical microscopy. The rest of the sample in the excess container can be re-analyzed with magnetic microspheres that are functionalized with another type of antibody or with fluorescent staining for other applications such as flow cytometry or confocal microscopy. Prior to each printout, the bio-ink is gently re-suspended with a pipette or vortex to ensure a homogenous dispersion of cells and beads in the buffer. Several printouts from a given mouse spleen are done with the prepared bio-ink by repeating the aforementioned process. Twelve different mouse spleen lymphocyte populations were tested during this study. Each spleen had eight to ten printouts and each printed sample had up to 15 images taken for cell counting purposes. Figure 3.4.1 is a diagram depicting an example of the printing and cell counting process for a single spleen lymphocyte population obtained from one mouse.

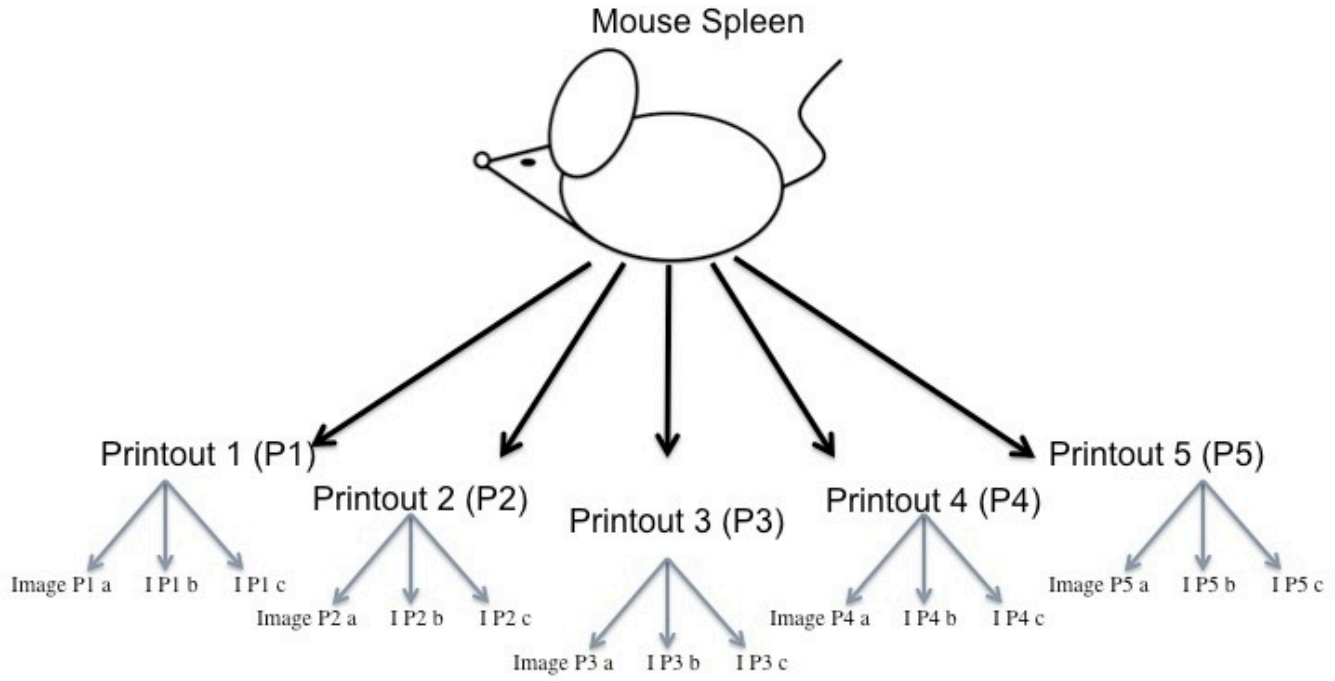

Figure 3.4.1: Example of Printing and Cell Counting Process

3.5 Cell Count

The images taken from the printed samples were used to obtain a count of the magnetically isolated cells and evaluate the instrument's sorting performance. Digital image analysis was performed by the use of FIJI, an open source image processing package based on Image J that was developed by the National Institute of Health. The magnetically bound cells in the digital image were counted with the Point Picker plugin. The average cell count from the images for each slide was calculated and used to estimate the CD4+ cell population within the spleen sample. The CD4+ cell count from each spleen along with the initial cell counts obtained from the hemocytometer were then used to calculate the estimated %CD4+ value for the entire lymphocyte content in each spleen sample. Minitab 15 Statistical Software (Minitab Inc., State College, PA) was used for statistical analysis to determine the validity of the printed cell count results in comparison to the actual cell counts obtained from flow cytometry and the use of a hemocytometer [4, 9].

In order to estimate the CD4+ cell count for each splenocyte population, the volume of a given image must be known. A volume factor was obtained by using the proportion in Figure 3.5.1. In this calculation, A_1 is the average CD4+ cell count out of the digital images for a given spleen. Since the images represent a physical volume that is being viewed, A_1 is divided by x, the volume of the image in µl, to give a cell concentration. This can be equalized to the actual CD4+ cell concentration in cells/ µl. The unknown variable can then be solved, which in this case is x, the volume of a given image. This calculation was done for every splenocyte population. The volume factor was determined by taking the average of the minimum and maximum values in order to avoid any kind of bias toward the data. The splenocyte populations that provided the maximum and minimum volume factor values were removed from the rest of the study to, again, avoid any bias in the data. It should be noted that both Spleen 9 and Spleen 10 had the minimum volume factor value. A coin toss was done in order to randomly choose which set of data would not be used in the rest of the study. In addition, Spleen 2, 3, and 4 were not included in this calculation because they were not tested with flow cytometry. The estimated CD4+ cell count from the printouts for each remaining splenocyte population was then calculated by using the ratio in Figure 3.5.2. In this case, the "Estimated" value is the unknown value and can be solved for by using the average CD4+ cell count in the digital images for a given splenocyte population and the volume factor, x.

$$\frac{A_1}{x} = \frac{Actual\ CD4+\ cells}{1\ ml = 1000\ \mu l}$$

Figure 3.5.1: Volume Factor

$$\frac{A_1}{x} = \frac{Estimated}{1\ ml = 1000\ \mu l}$$

Figure 3.5.2: Estimated CD4+ Lymphocyte Count from Printouts

3.6 Fluorescent Stain Analysis

The presence of CD4+ T cells was confirmed by fluorescent staining for Confocal Microscopy and Flow Cytometry analysis. The cells in the excess container along with a control sample of cells from the same spleen were stained with 1 µg anti-mouse CD4-FITC (Invitrogen, Carlsbad, CA) for 30 minutes. After a final wash, samples were fixed in 500 µl of 1 % formaldehyde following staining (Sigma-Aldrich). Negative and positive control samples of unstained and stained cells were used for reference standards in the analysis. Some bio-ink samples were fluorescently stained prior to being printed so the slides could be examined with the confocal microscope. Confocal Microscopy was done with a Nikon D-Eclipse C1 *Si* (Nikon Instruments Inc., Melville, NY). Flow cytometry analyses were performed using a Gallios Flow Cytometer (Beckman Coulter, Miami, FL). The flow cytometry results were interpreted with FlowJo 7.6.5 Flow Cytometry Analysis Software (Tree Star Inc., Ashland, OR) and sample gating was done on the densest area on the sample population.

Chapter 4

Results and Discussion

4.1 Proof of Concept Study

The optimal printing parameters to achieve sample sorting were determined in the proof of concept study. The colored microspheres were successfully sorted from the magnetic microspheres on polyester-based polymer slides created from the 3M PP2500^{TM} Transparency Film for Copiers (3M, St. Paul, MN) with the magnet 5 cm from the cartridge nozzle and the platform 18.5 cm above the base of the instrument in the horizontal printing position. Under these constraints, the blue colored non-magnetic microspheres would clearly segregate from the red magnetic microspheres. The magnetic microspheres were affected by the field of the permanent magnets on the customized platform and remained immobilized at the center of the slide which is the printing target area. Due to the hydrophobic nature of the polymer slide, the blue microspheres would continue to be affected by their momentum from the force of ejection and gravity so that they would slip from the middle to the bottom edge of the slide (Fig. 4.1.1). The blue microspheres could then be gently rinsed with PBS into the excess container by using a pipette. The results from this study provided a foundation on which to test the cell sorting hypothesis with this system.

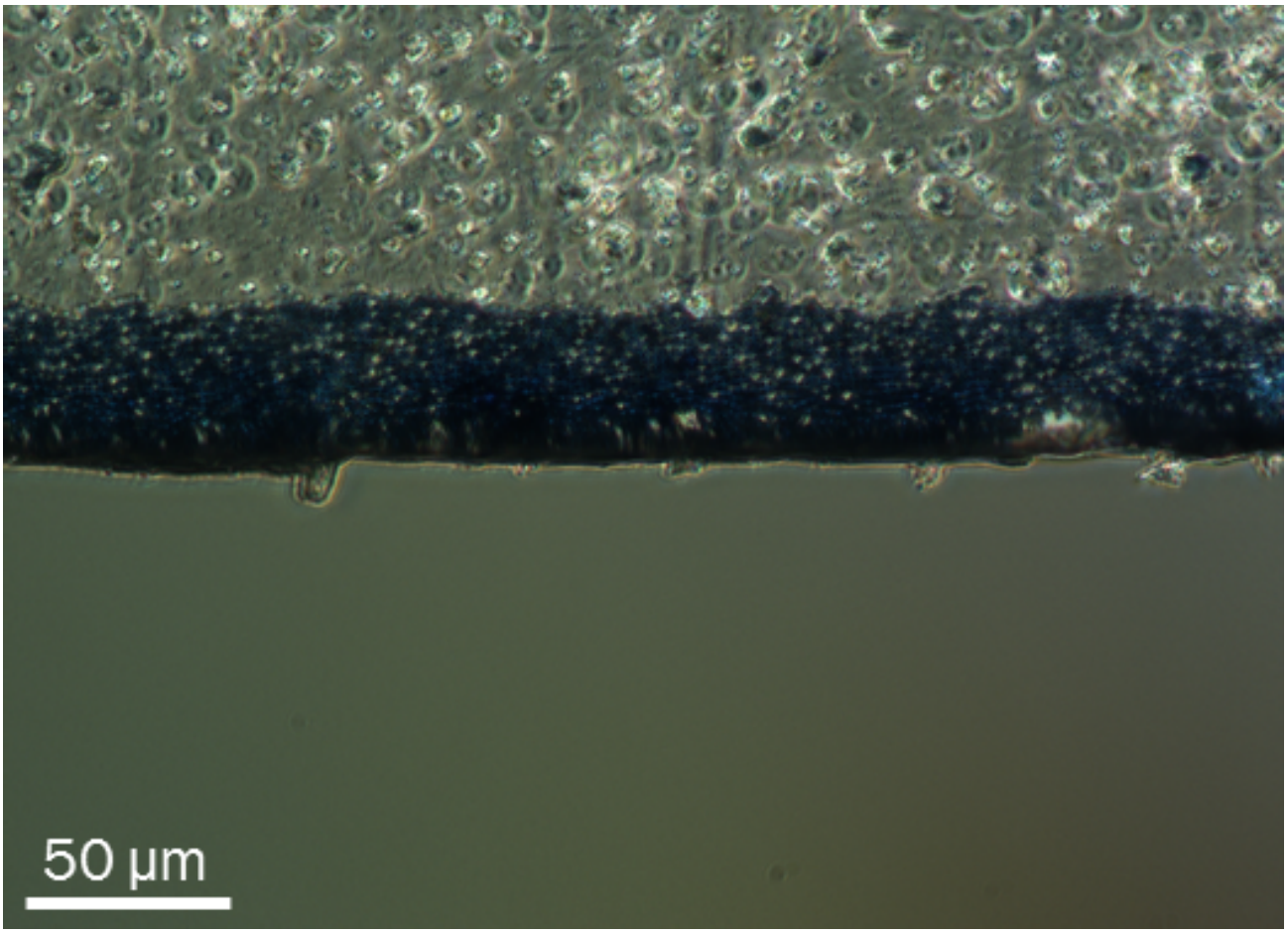

Figure 4.1.1: Separation of the Non-magnetic and Magnetic Microspheres on PET slide

4.2 Confocal Microscopy

Confocal microscopy was used to further confirm the presence of CD4+ lymphocytes in the spleen samples. Figure 4.2.1 shows the fluorescing cells that were stained with the CD4+ anti-mouse FITC fluorescent marker. A part of the Spleen 5 sample was stained with the CD4+ FITC marker prior to being bound with the magnetic microspheres. This part of the sample was then printed and viewed with confocal microscopy. Figure 4.2.2 shows the bright field images above the confocal microscopy images for the stained cells bound to the magnetic microspheres (a) and the excess container (b). Almost no fluorescing cells were detected in the excess container.

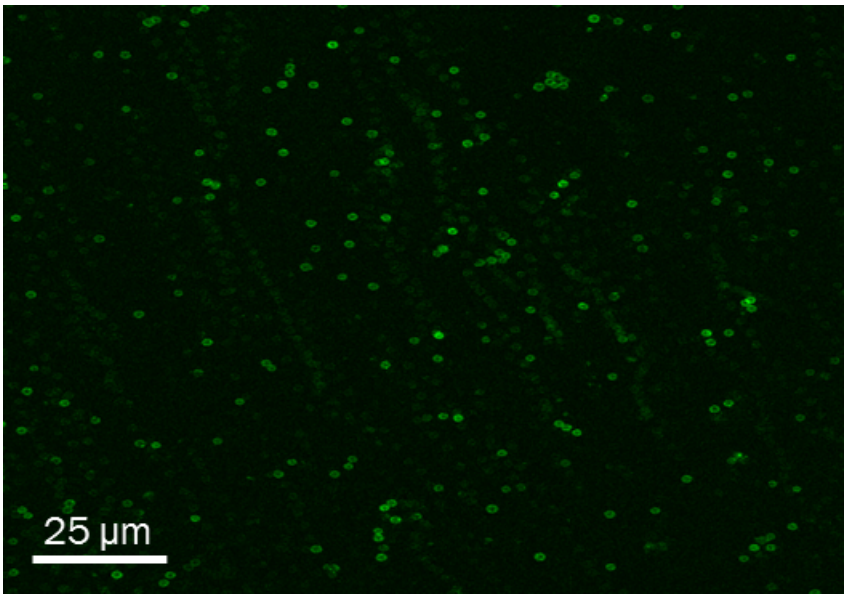

Figure 4.2.1: Confocal Microscopy of CD4+ lymphocytes from mouse Spleen 2 (FITC)

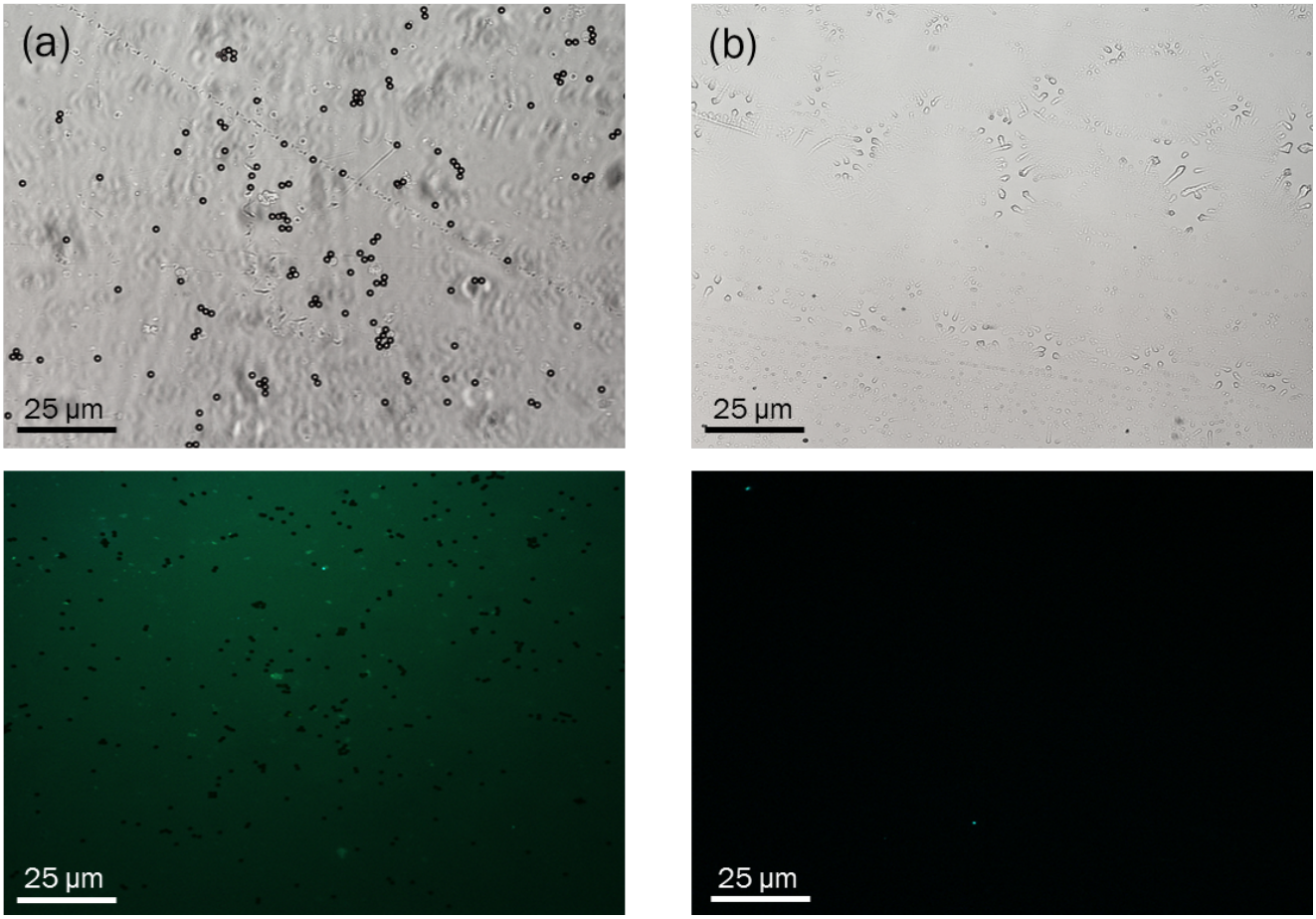

Figure 4.2.2: Confocal Microscopy (a) Printed Sample (b) Excess Container

4.3 Flow Cytometry Analysis

Table 4.3.1 summarizes the flow cytometry results for the CD4+ lymphocyte content in each mouse spleen that was used in the cell printing tests. The average lymphocyte content for the mouse spleens was about 24%. The average %CD4+ value was used for Spleen 2, 3, and 4 since no flow cytometry analysis was performed. Figure 4.3.1 demonstrates the flow cytometry results for Spleen 7, the column on the right shows a density plot of the cells and the left column shows a histogram which indicates the CD4+ content in the sample. It should be noted that all tests were done with the same settings to ensure they could be compared. Figure 4.3.1 (a) and (b) show test results of the negative control sample. Figure 4.3.1 (c),(d) show the results for the positive control which gives the value for the

%CD4+ lymphocyte content in Spleen 7. Figure 4.3.1 (e),(f) demonstrate the results for the cells caught in the excess container while printing the bio-ink created from Spleen 7. The flow cytometry results for the excess container verified the presence of cells in the excess container. Within the excess container population, only a small amount of cells were found to be CD4+ lymphocytes (Figure 4.3.1(f)). Table 4.3.2 shows the flow cytometry results on the amount of CD4+ cells in the excess container population for each spleen. This value should not be mistaken with the CD4+ cells in the spleen lymphocyte population shown in Table 4.3.1. The total amount of CD4+ cells printed during testing for each spleen was calculated by knowing the loading volume for each printout, the number of printouts, the cell concentration, and the %CD4+ cells in the spleen lymphocyte population. Then the percentage of CD4+ cells from the total amount of CD4+ cells that were printed was calculated. The last column in Table 4.3.2 provides these values and demonstrates that the amount of CD4+ cells that land in the excess container during testing are insignificant and most CD4+ cells land on the polymer substrate. This is due to the fact that, at most, a tenth of a percent of the total CD4+ cells printed during testing land in the excess container. This is actually in compliance with the dynabead manufacturer specifications which indicate the cell isolation purity to be greater than or equal to 95%. Thus, the CD4+ cells in the excess container do not have to be considered when doing cell counts. The flow cytometry results for the excess container also show that some dynabeads are caught in the excess container (Fig. 4.3.1(e)). Figure 4.3.2 shows flow cytoemtry results for pure, non-bound CD4+ dynabeads which were tested under the same settings as the mouse spleen lymphocytes and excess containers. These results were used to verify the presence of the dynabeads detected in the excess containers because they appear to be about the same size and granularity in both Figure 4.3.2 and Figure 4.3.1(e).

Table 4.3.1: Flow Cytometry Results for Mouse Spleens

	Actual Cell Concentration (cells/ml)	Flow Cytometry %CD4+ Cells
Spleen 1	12,260,000	24.34
Spleen 2	13,140,000	n/a
Spleen 3	2,056,000	n/a
Spleen 4	1,876,000	n/a
Spleen 5	8,000,000	22.72
Spleen 6	10,700,000	16.35
Spleen 7	4,890,000	22
Spleen 8	3,660,000	25.9
Spleen 9	12,200,000	26.35
Spleen 10	12,300,000	26.75
Spleen 11	10,100,000	24.2
Spleen 12	11,500,000	24.9
	Average	**23.72**

*Average %CD4+ value for Flow Cytometry used

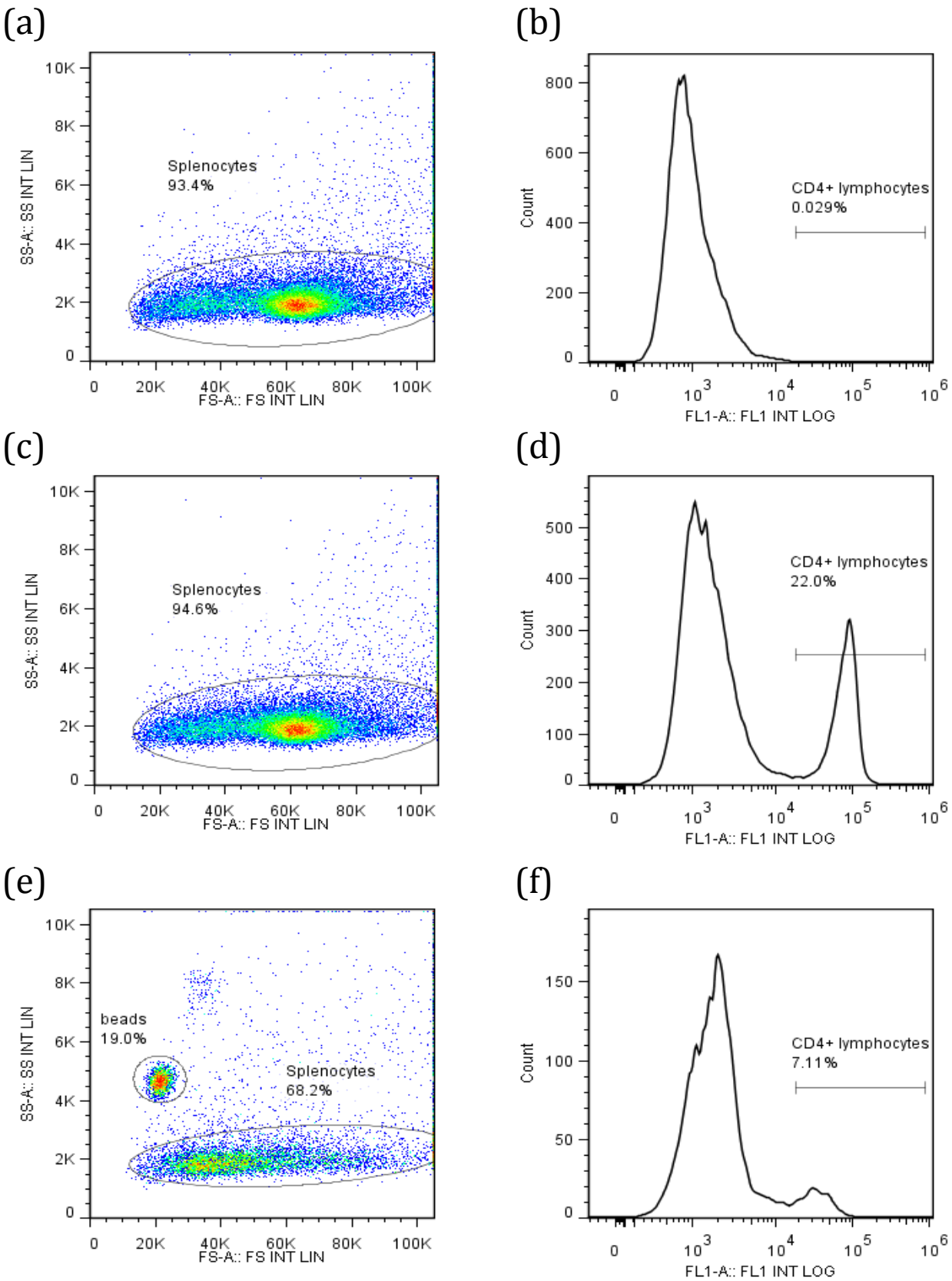

Figure 4.3.1: Flow Cytometry Analysis of Spleen 7

	Total CD4+ Cells Printed	CD4+ Cells in Excess Container	Printed %CD4+ cells in Excess Container
Spleen 1	298,408	4	0.001
Spleen 2	n/a	n/a	n/a
Spleen 3	n/a	n/a	n/a
Spleen 4	n/a	n/a	n/a
Spleen 5	68,196	44	0.06
Spleen 6	419,868	42	0.01
Spleen 7	258,192	491	0.19
Spleen 8	208,547	74	0.04
Spleen 9	771,528	947	0.12
Spleen 10	789,660	225	0.03
Spleen 11	391,072	314	0.08
Spleen 12	572,700	771	0.13

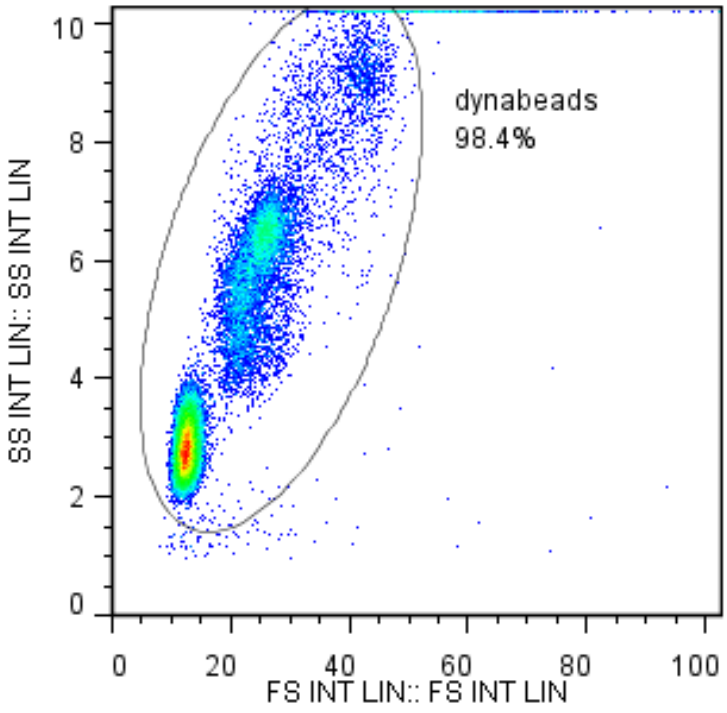

Figure 4.3.2: Flow Cytometry Density Plot of CD4+ Dynabeads

4.4 Cell Count

Several pictures were taken of each printed sample for Spleen 1 through Spleen 12 and the cells bound to the magnetic beads in each image were counted in order to estimate the CD4+ lymphocyte count. Figure 4.4.1(a) is an example of the images obtained from the printed samples and Figure 4.4.1(b) shows a higher magnification picture of the bead-bound cell from the previous image. In the cell counting process, Figure 4.4.1(a) is considered to only have one CD4+ lymphocyte and the count for this picture is one. Table 4.4.1 shows the image volume values in μl for each splenocyte population and Table 4.4.2 shows the calculation of the actual volume factor, x, which is 0.0018 μl. Table 4.4.3 summarizes the total cell concentration obtained from the hemocytometer and the CD4+ cell concentration determined by flow cytometry for each spleen. In addition, this table shows the CD4+ cell concentration and %CD4+ cells that were estimated from the printed samples (the standard deviation values are presented in later tables). A one sample t-test with the mean of the printed cell counts, in cells/ml, tested against a hypothesized mean was performed on each mouse spleen population. Each spleen population is approximated to be a normal distribution. The hypothesized mean, in cells per milliliter, is the CD4+ cell count obtained from the total cell count and flow cytometry analysis. The test is based on a 95% confidence interval (CI) with the null hypothesis being: "The printed cell count will match the cell count from the hemocytometer and flow cytometry analysis". The results of the t-test are shown in Table 4.4.4. All of the lymphocyte populations except for Spleens 4 and 10 – 12 show a p-value above 0.05 which indicates their hypothesized means are within the 95% confidence interval. Thus, the null hypothesis can only be rejected for Spleens 4, 10, 11, and 12 while the rest demonstrate a reasonable cell count estimate. An ANOVA interval plot with a 95% confidence interval for the mean was created from estimated CD4+ cell counts from the printouts for every spleen (Fig. 4.4.2 (a) and (b)). This was compared with the actual CD4+ cell count that was determined with flow cytometry analysis and the initial cell count from the hemocytometer. The estimated CD4+ cell count from the printouts for

Spleens 1,2,3,6, 7, and 8 was determined to be valid since the cell count values based on flow cytometry and the hemocytometer fell within the interval of variance for the estimated cell counts. The large variance from the mean of the estimated CD4+ cell concentration could be the result of a similar type of variance in the cell counts from the digital images. A cell count from the digital images of the printouts can vary from zero CD4+ cells up to thirty CD4+ cells. The same statistical analysis was performed on the estimated %CD4+ values for each spleen to compare with the values given by the flow cytometer tests. Table 4.4.5 summarizes the t-test results for the estimated %CD4+ values and Figure 4.4.3 (a) and (b) demonstrates the ANOVA interval plot. The estimated %CD4+ values provided the same results as the estimated CD4+ cell counts. Again, Spleens 4 and 10 - 12 were the populations that did not show a p-value below 0.05 which indicates their hypothesized means are the only ones that are not within the 95% confidence interval. Thus, the null hypothesis is again rejected for those splenocyte populations while the rest demonstrate a reasonable estimated %CD4+ value. In the ANOVA interval plot with a 95% confidence interval, the estimated %CD4+ values from the printouts were determined to be valid since the flow cytometry values fell within the variance intervals for Spleens 1,2,3,6, 7, and 8.

Another common form of reporting CD4+ cell concentrations, especially in setting standards for HIV/AIDS diagnosis and monitoring, is cells/mm^3. The World Health Organization uses these units in their "Antiretroviral Therapy for HIV Infection in Adults and Adolescents: Recommendations for a Public Health Approach" manual which states that antiretroviral therapy should begin when a patient has less than or equal to 350 CD4+ lymphocytes per cubic millimeter. Table 4.4.6 demonstrates the estimated cell concentrations from the printouts for each spleen in these units.

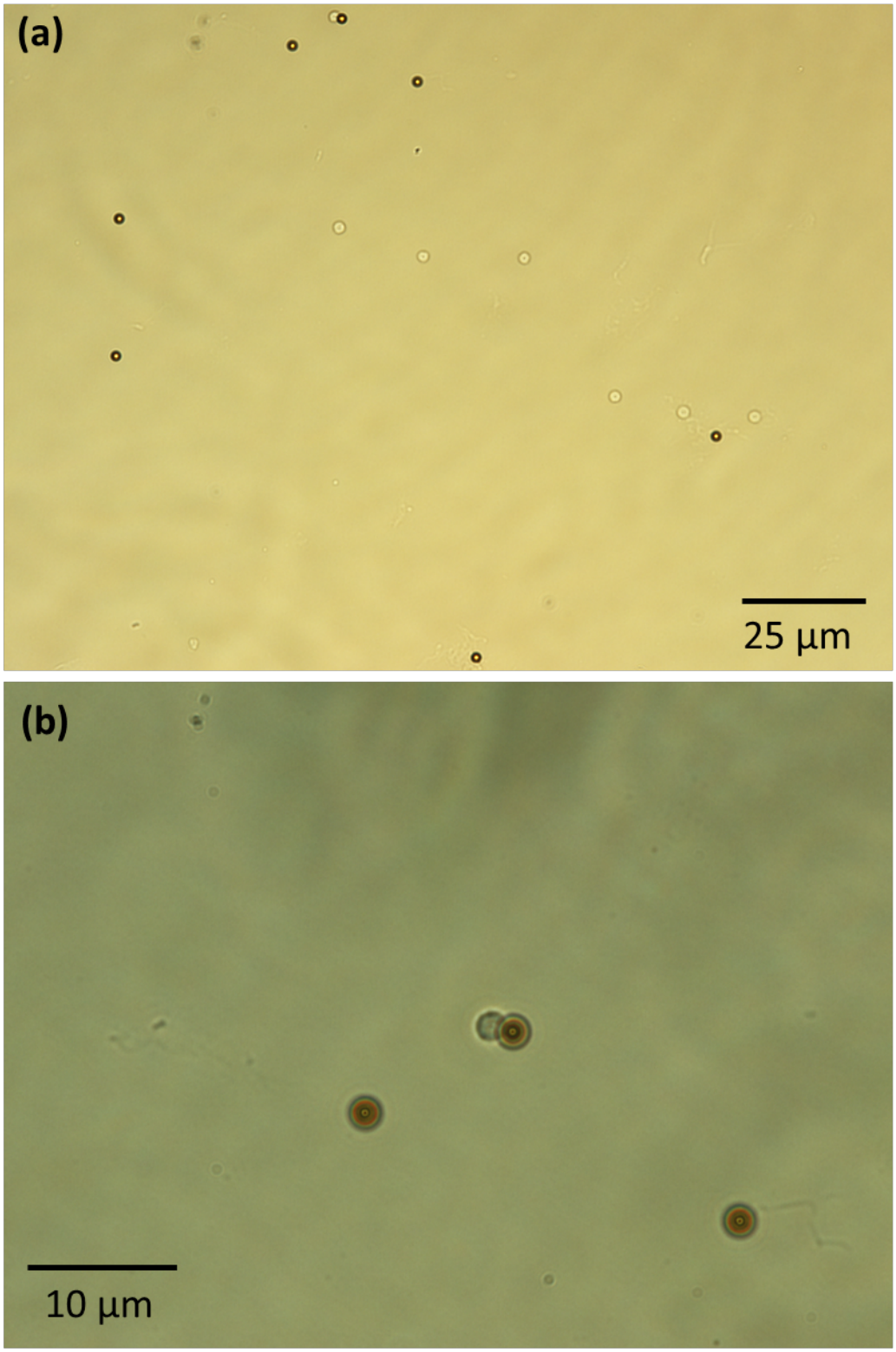

Figure 4.4.1: Example of Image from Printed Samples

Table 4.4.1: Volume Estimate

	Average CD4+ Cell Count per Image	Actual CD4+ Cell Concentration (cell/ml)	Volume Estimate (µl)
Spleen 1	3	2,881,100	0.0010
Spleen 5	5	1,880,000	0.0027
Spleen 6	2.13	1,749,450	0.0012
Spleen 7	2.10	1,075,800	0.0020
Spleen 8	1.89	947,940	0.0020
Spleen 9	2.46	3,214,700	0.0008
Spleen 10	2.51	3,290,250	0.0008
Spleen 11	2.86	2,444,200	0.0012
Spleen 12	3.34	2,863,500	0.0012

Table 4.4.2:Volume Factor

Spleen 9	Min	0.0008
Spleen 5	Max	0.0027
	Average (Volume Factor)	0.0018

Table 4.4.3: Cell Count Summary

	Actual Cell Concentration (cells/ml)	Flow Cytometry %CD4+ Cells	Actual CD4+ Cell Concentration (cells/ml)	Estimated CD4+ Cell Concentration (cells/ml)	Estimated %CD4+ Cells
Spleen 1	12,260,000	24.34	2,881,100	1,666,667	13.59
Spleen 2	13,140,000	n/a*	3,116,808	4,841,270	36.84
Spleen 3	2,056,000	n/a*	487,683	740,741	36.03
Spleen 4	1,876,000	n/a*	444,987	287,037	15.30
Spleen 6	10,700,000	16.35	1,749,450	1,181,746	11.04
Spleen 7	4,890,000	22	1,075,800	1,165,657	23.84
Spleen 8	3,660,000	25.9	947,940	1,047,531	28.62
Spleen 10	12,300,000	26.75	3,290,250	1,391,975	11.32
Spleen 11	10,100,000	24.2	2,444,200	1,586,806	15.71
Spleen 12	11,500,000	24.9	2,863,500	1,855,556	16.14
	Average	**23.72**			

*Average %CD4+ value for Flow Cytometry used

Table 4.4.4: T-test Results for CD4+ Printed Cell Counts

	Hypothesized Mean	N	Mean	StDev	95% CI	T	P
Spleen 1	2881100	3	1666667	962250	(-723696, 4057029)	-2.19	0.16
Spleen 2	3116808	7	4841270	3831780	(1297464, 8385075)	1.21	0.272
Spleen 3	487683	6	740741	672811	(34669, 1446813)	0.94	0.391
Spleen 4	444987	6	287037	142364	(137635, 436439)	-2.65	0.046
Spleen 6	1749450	7	1181746	818383	(424868, 1938624)	-1.84	0.116
Spleen 7	1075800	9	1165657	748228	(662990, 1668323)	0.4	0.699
Spleen 8	947940	9	1047531	625550	(566691, 1528371)	0.48	0.646
Spleen 10	3290250	9	1391975	1005483	(619093, 2164858)	-5.66	0
Spleen 11	2444200	8	1586806	820106	(901179, 2272432)	-2.96	0.021
Spleen 12	2863500	9	1855556	1010703	(1078661, 2632450)	-2.99	0.017

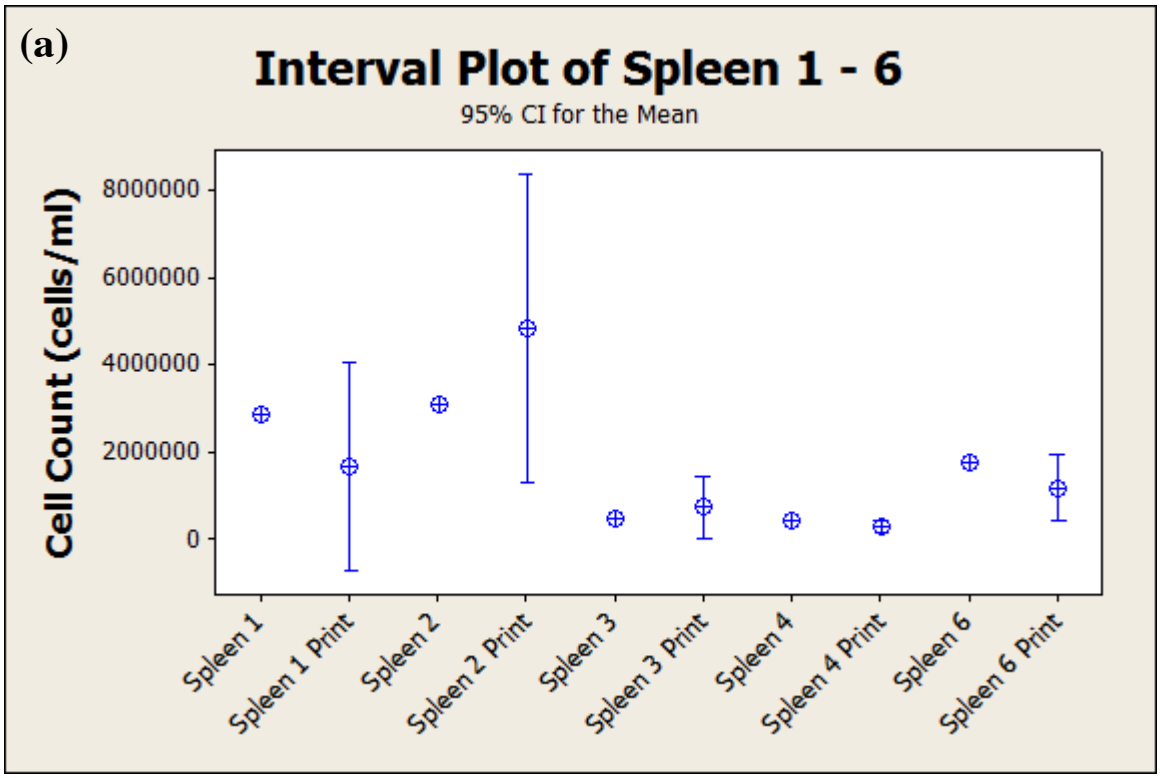

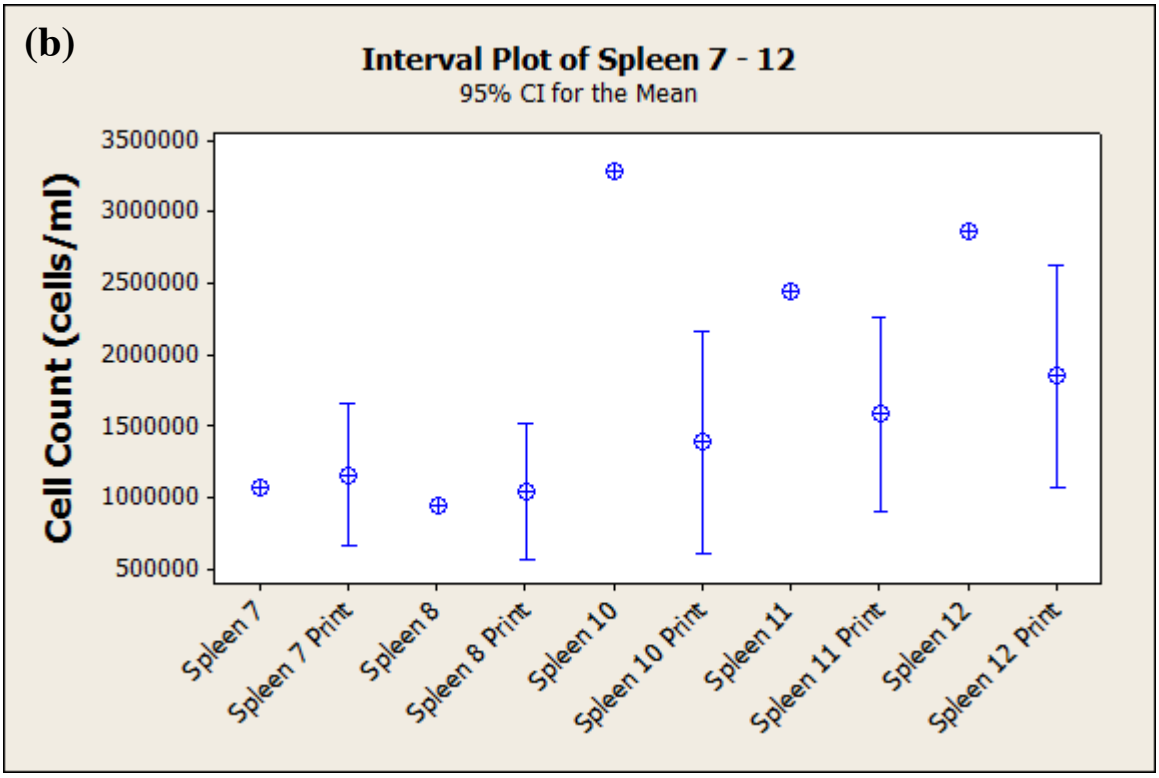

Figure 4.4.2: Interval Plot of CD4+ Printed Cell Counts with 95% CI Compared to Actual Cell Counts

Table 4.4.5: T-test Results for %CD4+ Printed Cell Counts

	Hypothesized Mean	N	Mean	StDev	95% CI	T	P
Spleen 1	24.34	3	13.59	7.85	(-5.90, 33.09)	-2.37	0.141
Spleen 2	23.72	7	36.8	29.2	(9.9, 63.8)	1.19	0.279
Spleen 3	23.72	6	36	32.7	(1.7, 70.4)	0.92	0.399
Spleen 4	23.72	6	15.3	7.59	(7.34, 23.26)	-2.72	0.042
Spleen 6	16.35	7	11.04	7.65	(3.97, 18.12)	-1.84	0.116
Spleen 7	22	11	23.84	15.3	(13.56, 34.12)	0.4	0.699
Spleen 8	25.9	9	28.62	17.09	(15.48, 41.76)	0.48	0.646
Spleen 10	26.75	9	11.32	8.17	(5.03, 17.60)	-5.66	0
Spleen 11	24.2	8	15.71	8.12	(8.92, 22.50)	-2.96	0.021
Spleen 12	24.9	9	16.14	8.79	(9.38, 22.89)	-2.99	0.017

(a)

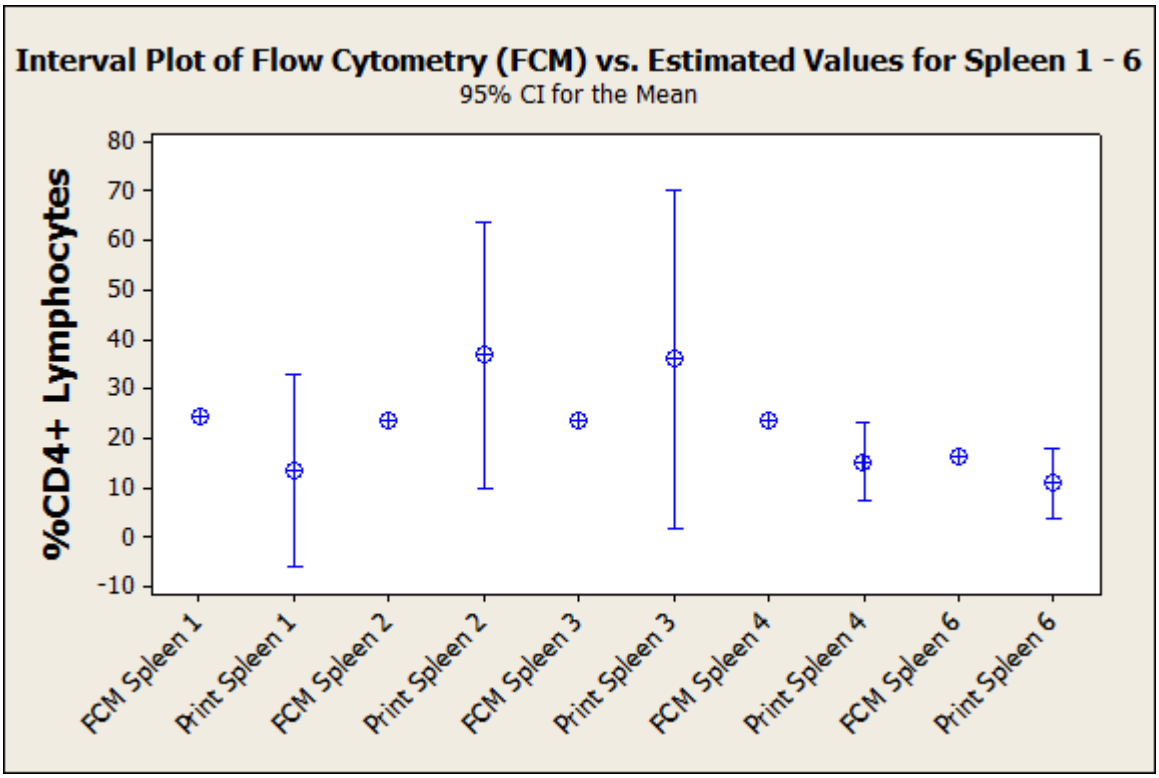

(b)

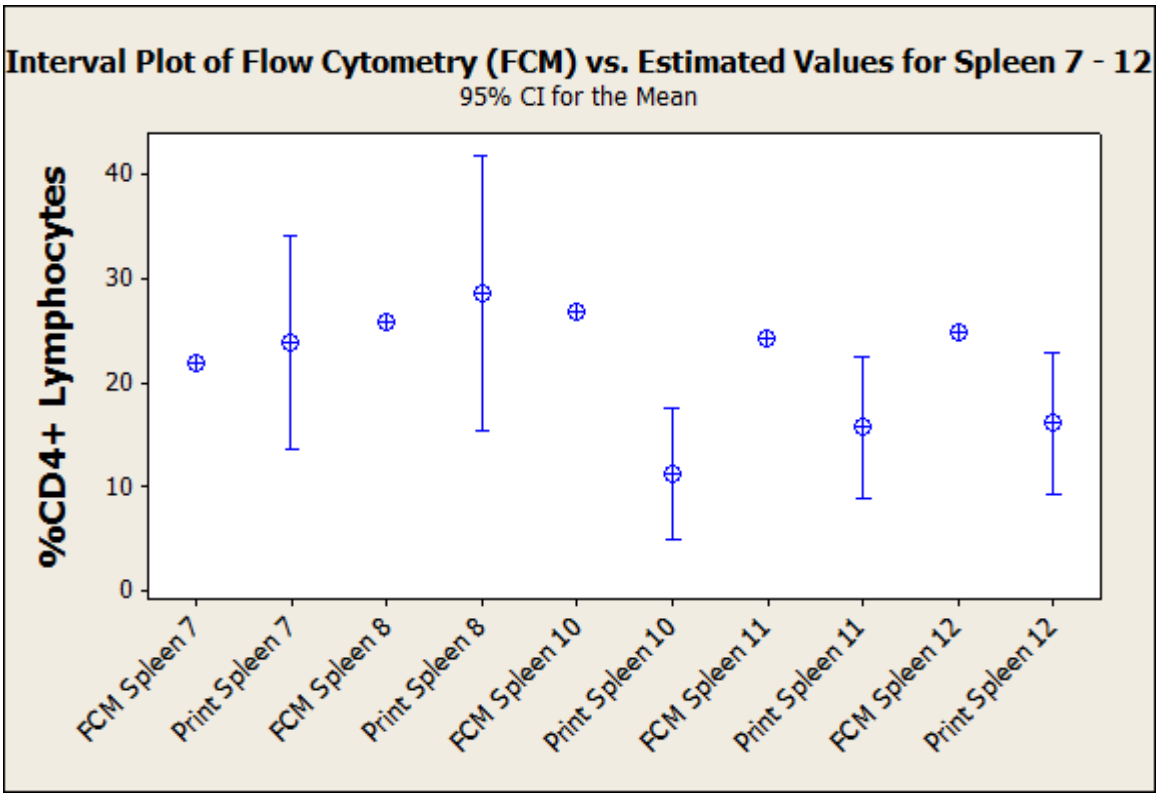

Figure 4.4.3: Interval Plot of Flow Cytometry %CD4+ Values vs. Printed Values with 95% Confidence Interval

Table 4.4.6: Cell Concentration in Cells per Cubic Millimeter

	Actual Cell Concentration (cells /mm^3)	Actual CD4+ Cell Concentration (cells /mm^3)	Estimated CD4+ Cell Concentration (cells /mm^3)
Spleen 1	12,260	2,881	1,667
Spleen 2	13,140	3,117	4,841
Spleen 3	2,056	488	741
Spleen 4	1,876	445	287
Spleen 6	10,700	1,749	1,182
Spleen 7	4,890	1,076	1,166
Spleen 8	3,660	948	1,048
Spleen 10	12,300	3,290	1,392
Spleen 11	10,100	2,444	1,587
Spleen 12	11,500	2,864	1,856

Chapter 5

Summary and Conclusions

The goal of this study was to create an inexpensive, portable cell sorting technique for low resource settings by combining inkjet printing and immunomagnetic separation technology. This was achieved through the modification of a commercially available thermal inkjet printer and creation of an optimized printing process to magnetically sort cells. The cell counting protocol was optimized to be simple yet accurate and its reliability was assessed by several analytical tools. The proof-of-concept study demonstrated that this novel printing system was capable of sorting magnetic, micron-sized particles from a mixed sample. Therefore, the study progressed to isolating a specific type of lymphocyte, CD4+ helper T cells, that are commonly affected by chronic diseases such as HIV/AIDS from a mixed lymphocyte population obtained from mouse spleens. Confocal microscopy confirmed the presence of the CD4+ cells and their attachment to the dynabeads. This validated the use of protein specific attachment of magnetic microspheres to the lymphocytes for cell sorting. Flow cytometry analysis, the standard method of cell sorting and counting, also confirmed the presence of CD4+ lymphocytes and provided an accurate estimate of how many were present in the spleen cell population. In addition, flow cytometry verified the presence of cells in the excess container that were being sorted from the rest of the bio-ink. The presence of the CD4+ cells in the excess container along with dynabeads was detected, however, this was proven to be a miniscule amount that was not significant to the cell count accuracy. Therefore, it can be concluded that about 99% of the printed CD4+ cells were being sorted from the sample and remained on the polymer slide while the rest of the sample fell into the excess container. Statistical analysis demonstrates that most of the printed samples provide an accurate estimate of the CD4+ cell count.

It is important to note that in many low resource settings microscopes that can take digital images are unavailable. At this stage, the minimum requirements for this cell sorting system to work in the resource poor settings, aside from basic supplies and an operator, are a source of electricity, a simple light microscope, and a hemocytometer. Further improvements are needed to prepare it for situations where the minimum requirements cannot be met. In its preliminary stages of development, however, this prototype has demonstrated great potential as an inexpensive point-of-care diagnostic tool in medically underserved areas. As a result of this study, testing this system on human lymphocyte samples is now justified and its usefulness can be expanded to monitoring the progression of other chronic diseases.

References

1. Balakrishman, P.,Solomon, S. (2005). Low-cost monitoring of HIV infected individuals on highly active antiretroviral therapy (HAART) in developing countries. *Indian J Med Res*, *121*, 345-355.
2. Beeson, R. (1998). Thermal (TIJ) or Piezo? Who Cares? *IMI 7th Annual Ink Jet Printing Conference*,.
3. Benjamini, E., Coico, R.; Sunshine, G. (2010). *Immunology: A Short Course* (6th ed.). Danvers, MA: Wiley-Liss, Inc.
4. Berendsen, H. (2011). *A Student's Guide to Data and Error Analysis.* Cambridge, UK: Cambridge University Press.
5. Calvert, P. (2007). Printing Cells. *Science*, *318*, 208.
6. Carraher, C. E. (2007). *Introduction to Polymer Chemistry.* Boca Raton: CRC Press Taylor and Francis Group.
7. Chen, P.-H., Chen, Wen-Cheng; Chang, S.H. (1997). Bubble growth and ink ejection process of a thermal ink jet printhead. *International Journal of Mechanical Science*, *39*(6), 683-695.
8. Cui, X., Boland, T. (2009). Human microvasculature fabrication using thermal inkjet printing technology. *Biomaterials*, *30*, 6221-6227.
9. Dunn, J. (2009). *Basic Statistics: a primer for the biomedical sciences.* Hoboken, NJ: John Wiley & Sons.
10. Flint, A. (2011). *HIV/AIDS in Sub-Saharan Africa: Politics, Aid, and Globalization.* London, UK: Palgrave Macmillan.
11. Furlani, E. P. (2001). *Permanent Magnet and Electromechanical Devices.* San Diego: Academic Press.

12. Furlani, E. P., Sahoo, Y.; Ng, K.C.; Wortman, J.C.; Monk, T.E. (2007). A model for predicting magnetic particle capture in a microfluidic bioseparator. *Biomedical Microdevices*, *9*, 451-463.
13. Gaudernack, G., Leivestad, Torbjorn; Ugelstad, John; Thorsby, Erik. (1986). Isolation of pure functionally active CD8+ T cells. *Journal of Immunological methods*, *90*, 179-187.
14. Gillis, S., Scheid, M.; Watson, J. (1980). Biochemical and Biologic Characterization of Lymphocyte Regulatory Molecules. *The Journal of Immunology*, *128*(6), 2570-2578.
15. Gorman, M.,Zijenah, L. (2008). CD4 T Cell Measurements in the Management of Antiretroviral Therapy - A Review with an Emphasis on Pediatric HIV-infected Patients. *Cytometry Part B*, *748*, S19-S26.
16. Gupta, A., Gupta, M. (2005). Synthesis of surface engineering of iron oxide nanoparticles for biomedical applications. *Biomaterials*, *26*, 3995-4021.
17. Hafeli, U. (1997). *Scientific and Clinical Applications of Magnetic Carriers*. Proceedings from International Conference on Scientific and Clinical Applications of Magnetic Carriers, New York, NY.
18. Hermanson, G. T. (2008). *Bioconjugate Techniques.* Burlington, MA: Elsevier Inc.
19. Hibbeler, R. C. (2007). *Engineering Mechanics Dynamics* (11 ed.). Upper Saddle River: Pearson Prenstice Hall.
20. Ho, V., Barcza, A.; Chen, R. (2009). The precise control of cell labelling with streptavidin paramagnetic particles. *Biomaterials*, *30*, 6548-6555.
21. Hook, A., Anderson, D.; Langer, R. (2010). High throughput methods applied in biomaterial development and discovery. *Biomaterials*, *31*, 187-198.
22. Invitrogen-dynal. (2011). Magnetic properties of MyOne dynabeads.
23. Kortum-Richards, R. (2010). *Biomedical Engineering for Global Health.* New York, NY: Cambridge University Press.

24. Kyewski, B., Payer, E. (2005). *CD4+ and CD25+ Regulatory T Cells: Origin, Function, and Therapeutic Potential* (293). Germany: Springer-Verlag Berlin Heidleberg.

25. Logan, D. L. (2002). *A First Course in the Finite Element Method* (3 ed.). Pacific Grove: Wadsworth Group.

26. Macey, M. (2007). *Flow Cytometry Principles and Applications.* Totowa, NJ: Humana Press Inc.

27. McCraig, M. (1977). *Permanent Magnets in Theory and Practice.* New York, NY: John Wiley & Sons Inc.

28. Milteni, S., Muller, W.; Weichel, W. (1990). High Gradient Magnetic Cell Separation with MACS. *CYTOMETRY*, *11*, 231-238.

29. Mironov, V., Visconti, Richard; Kasyanov, Vladmir. (2009). Organ printing: Tissue spheroids as building blocks. *Biomaterials*, *30*, 2164-2174.

30. Molday, R. (1982). Immunospecific ferromagnetic iron-dextran reagents for the labeling and magnetic separation of cells. *Journal of Immunological methods*, *52*, 353-367.

31. Nakamura, M., Kobayashi, A.; Takagi, F. (2005). Biocompatible Inkjet Printing Technique for Designed Seeding of Individual Living Cells. *Tissue Engineering*, *11*, 1658.

32. Norotte, C., Marga, F.; Niklason, L. (2009). Scaffold-free vascular tissue engineering using bioprinting. *Biomaterials*, *30*, 5910-5917.

33. Pamme, N., Manz, A. (2004). On-chip free-flow magnetophoresis: Continuous Flow Separation of Magnetic Particles and Agglomerates. *Analytical Chemistry*, *76*, 7250-7256.

34. (2000). *T Cell Protocols: Development and Activation.* Totowa, NJ: Humana Press, Inc.

35. Rivron, N., Rouwkema, J.; Truckenmuller, R. (2009). Tissue assembly and organization: Developmental mechanisms in microfabricated tissues. *Biomaterials*, *30*, 4851-4858.

36. Rosen, S., O'Farrell, Brendan. (2011). Point of Care Diagnostics For Emerging Disease Threats. *Kalorama Information Market Intelligence Report*,.

37. Roth, E. A., Xu, T.; Das, M.; Gregory, C.; Hickman, J.J.; Boland, T. (2004). Inkjet printing for high-throughput cell patterning. *Biomaterials*, *25*, 3708-3715.

38. Sadava, D., Heller, Craig H.; Orians, Gordon H.; Purves, William K.; Hillis, David M. (2008). *Life: The Science of Biology* (8 ed.). Sinaur Associates, Inc.

39. Safarik, I., Safarikova, Mirka. (1999). Use of magnetic techniques for the isolation of cells. *Journal of Chromatography B*, *722*, 33-53.

40. Sax, P., Cohen, C.; Kuritzkee, D. (2008). *HIV Essentials* (2nd ed.). Jones and Bartlett Publishers, LLC.

41. Shechter, L., Wynstra, J.; Kurkjy, R. (1956). Glycidyl Ether Reactions with Amines. *Industrial and Engineering Chemistry*, *48*, 94-97.

42. Skomski, R. (2008). *Simple Models of Magnetism.* Oxford: Oxford University Press.

43. Spaldin, N. A. (2011). *Magnetic Materials.* Cambridge, UK: Cambridge University Press.

44. Thomas, T. E., Abraham, Sara J.R.; Otter, Alan J.; Blackmore, Ewart W.; Lansdorp, Peter M. (1992). High gradient magnetic separation of cells on the basis of expression levels of cell surface antigens. *Journal of Immunological methods*, *154*, 245-252.

45. Tsoukas, C. (2006). *Lymphocyte Signal Transduction* (576). Springer Science+Business Media.

46. U.S. Department of Health and Human Services, B. o. H. P. H. R. a. S. A. H. R. S. A.). (2012). Designated Health Professional Shortage Areas Statistics.

47. Veeramachaneni, U., Carroll, Lloyd. (2007). Magnetic Particle Motion in a Gradient Field. *COMSOL Conference Proceedings*,.

48. Whitford, D. (2005). *Proteins Structure and Function.* Chichester, England: John Wiley and Sons Ltd.

49. Wilhelm, C., Gazeau, F. (2008). Universal cell labelling with anionic magnetic nanoparticles. *Biomaterials*, *29*, 3161-3174.

50. World Health Organization, W. H. O. (2010). *Antiretroviral therapy for Hiv Infection in Adults and Adolescents: Recommendations for a Public Health Approach.* Austria: WHO Press.

51. World Health Organization, W. H. O. (2011). *World Health Statistics 2011.* France: WHO Press.

52. Wu, I.-D., Chang, Feng. (2007). Determination of the interaction within polyester-based solid polymer electrolyte using FTIR spectroscopy. *Polymer*, *48*, 989-996.

53. Xu, T., Gregory, Cassie; Molnar, Peter; Boland, Thomas. (2006). Viablility and electrophysiology of neural cell structures generated by the inkjet printing method. *Biomaterials*, *27*, 3580-3588.

54. Xu, T., Jin, Joyce; Gregory, Cassie; Hickman, James; Boland, Thomas. (2005). Inkjet printing of viable mammalian cells. *Biomaterials*, *26*, 93-99.

55. Zhou, H., Gue, A. (2010). Simulation model and droplet ejection performance of a thermal-bubble microejector. *Sensors and Actuators B: Chemical*, *145*, 311-319.

Vita

Sylvia Natividad received a B.Sc . in Metallurgical and Materials Engineering in May 2010 at The University of Texas at El Paso (UTEP) and is currently in the M.S. program in the Department of Metallurgical and Materials Engineering. She works as a graduate research assistant in the Printed Biomaterials Lab in the Metallurgy Department at UTEP in Dr. Boland's research group. During her graduate study for the M.S. program, she also worked in the Department of Biomedical Sciences in The Center of Excellence for Infectious Diseases at Texas Tech University Health Sciences Center in Dr. Zeng's lab. Her research experience includes Nb-based high-temperature superalloys for aerospace applications, processing of ZrB2 UHTC's for thermal protection systems in aerospace vehicles, cell culture techniques, and inkjet printing for biomedical applications.

Permanent address: 10239 Sumatra St.
El Paso, TX 79925

This thesis/dissertation was typed by Sylvia L. Natividad.